Applied Physics Letters

Will flat optics appear in everyday life anytime soon?

Cite as: Appl. Phys. Lett. **118**, 100503 (2021); https://doi.org/10.1063/5.0039885
Submitted: 07 December 2020 . Accepted: 19 February 2021 . Published Online: 09 March 2021

Wei Ting Chen, and Federico Capasso

Applied Physics Letters PERSPECTIVE scitation.org/journal/apl

Will flat optics appear in everyday life anytime soon?

Cite as: Appl. Phys. Lett. **118**, 100503 (2021); doi: 10.1063/5.0039885
Submitted: 7 December 2020 · Accepted: 19 February 2021 ·
Published Online: 9 March 2021

Wei Ting Chen[a] and Federico Capasso[a]

AFFILIATIONS

Harvard John A. Paulson School of Engineering and Applied Sciences, Harvard University, Cambridge, Massachusetts 02138, USA

Note: This Paper is part of the APL Special Collection on Metastructures: From Physics to Applications.
[a]**Authors to whom correspondence should be addressed:** weitingchen@seas.harvard.edu and capasso@seas.harvard.edu

ABSTRACT

Flat optical components based on metasurfaces will appear in our daily life in the near future. Our discussion focuses on metasurface-based components consisting of sub-wavelength spaced dielectric nanostructures in the optical region. After an introduction to the underlying technology, the advantages of metasurfaces are highlighted and the efforts in the development of metasurface components is discussed. The metasurface not only promises a reduction in the size and complexity of optical components but also brings new functionalities. Examples of achromatic optical components, a full-Stokes metasurface camera, and a metasurface depth sensor with superior performance are highlighted. Finally, future trends and opportunities are discussed.

The Huygens principle describes the propagation of light by the sum of spherical wavelets forming a wavefront. When light impinges on an array of subwavelength-spaced nanostructures, known as metasurfaces,[1] each of them can be regarded as the source of a spherical wavelet. Intriguingly, the amplitude, phase, polarization, and even the dispersion of spherical wavelets can be mainly controlled by the geometric parameters rather than the material composition of nanostructures.[2,3] In this way, the wavefront can be molded at will to create flat optical components with superior performance, including multifunctional ones, or to structure light by shaping vector beams with full control of polarization that would otherwise require multiple optical components and are beyond the capabilities of spatial light modulators.[4] Metasurfaces, therefore, open many design degrees of freedom and become a disruptive platform for flat and compact optical components and systems[5–7] and emerging applications such as ultrafast light steering,[8] synchrotron radiation,[9] and quantum photon sources.[10]

These advances have greatly benefited from the rapid development of nanofabrication of large-scale[11,12] and low-loss dielectric metasurfaces.[13,14] A variety of high-efficiency metasurface components have been demonstrated from the ultraviolet to the mid-infrared regions, and large-scale manufacturing with mature deep ultraviolet projection immersion lithography on 12-in wafer,[15,16] the same technique used for computer chip manufacturing, has been reported. This places metasurfaces under the radar of leading technology companies. A recent incubator meeting on flat optics hosted by the Optical Society and widely attended by academia, industry, and government agencies and laboratories reviewed recent advances in flat optics.[17] Participating companies included 3M, Corning, Magic Leap, Facebook, Applied Materials, Lockheed Martin, Sony, Samsung, ZEMAX, SUSS MicroOptics, Lumotive, Temicon, Voxtel, Ball Aerospace & Technologies, PlanOpSim, and ams Sensors. Sony and Samsung are also supporting the development of metasurface components and systems.[18,19] Startup companies have emerged to exploit the game changing metasurface technology. Lumotive Inc. combines liquid crystal and silicon metasurfaces as an ultrafast and high-resolution Lidar for automotive vehicles,[20] Leia Inc. provides a wide-angle and glasses-free three-dimensional display based on the control of scattered light using nanostructures,[21] and Metalenz Inc. is developing metasurface lenses (metalenses) and cameras for high-volume consumer markets.[22] Metamaterial Technologies Inc. focuses on nanophotonics-related techniques and has widespread intellectual property portfolio.[23] Efforts from governments are ever-increasing. DARPA has started a five-year research program "Extreme Optics," and Australian Research Council has supported a new research center: ARC Center of Excellence for Transformative Meta-optical Systems, both aiming for revolutionary optical components. Flat metasurface optics is about to take off, as indicated by World Economic Forum as one of the top ten emerging technologies of 2019 and predicted by Lux Research for $10 billion USD market opportunity by 2030.[24]

It is, therefore, apparent to us that within a relative short time, flat metasurface components or even systems will appear in our daily

life. In the following paragraphs, we will illustrate the key differences between metasurface and conventional diffractive elements and highlight metasurface components and systems that cannot be realized by conventional means.

We start from comparing a 0.5-numerical-aperture (NA) TiO_2 metalens and its diffractive counterparts: a saw-tooth Fresnel lens and a multilevel diffractive lens. For simplicity, we focus on the optical property for the marginal rays passing through the edge of each lens. This allows us to approximate the local region of each lens as a grating. One can repeat this assumption to obtain the efficiency of a full lens following the method reported in Ref. 25. Shown in Figs. 1(a)–1(c) are unit cells at the lens edges. The metalens comprises TiO_2 nanopillars, while the saw-tooth Fresnel lens is composed of miniature prisms [Fig. 1(b)] and the multilevel diffractive lens [Fig. 1(c)] is a digitized version of the profile depicted in Fig. 1(b). Here, we chose Polymethyl methacrylate (PMMA) rather than TiO_2 as the composition material for the saw-tooth Fresnel lens and the multilevel diffractive lens because these lenses are typically made of polymers by gray-scale lithography or molding with an index of refraction close to that of PMMA.[26] From these schematic diagrams, one notices that their underlying physical mechanisms for imparting phase delay are different. In the metalens, the phase delay is tailored by varying the pillars' diameter, which locally changes the effective refractive index. Each nanopillar can be treated as a truncated waveguide: the smaller the diameter, the more the electric field leaks into the air, lowering its effective index. The phase delay can be calculated by

$$\varphi = \frac{2\pi}{\lambda} \cdot n_{eff} \cdot H, \tag{1}$$

where n_{eff}, λ,, and H are the effective index, incident wavelength, and nanopillar height. On the contrary, both the saw-tooth Fresnel and the multilevel diffractive lens impart phase delays via different heights and their indices of refraction are equal to those of PMMA. A question to be answered is what advantage does the metalens provide by imparting phase delays by effective indices rather than heights. To answer this question, we performed full wave FDTD simulation to simulate the structures of Figs. 1(a)–1(c) with the periodic boundary condition. The colormaps from Figs. 1(d)–1(f) show the simulated transmission efficiency (referred to as efficiency hereinafter for simplicity), which is defined by the power of the -1 order diffracted beam [depicted by the solid green arrow in Fig. 1(a)] divided by the power of incident light, for the metalens, saw-tooth Fresnel lens, and multilevel diffractive lens, respectively. Here, we only focus on efficiency because their monochromatic aberrations, especially the coma aberration, can be corrected by placing an aperture at a distance of approximately one focal length away[27] or by a configuration of the metalens doublet.[28,29] Moreover, we note that spatial frequency engineering is also a promising approach to tackle monochromatic aberrations.[30,31] This approach is based on the design of each nanostructure in a way that its phase delay changes in a customized way with the angle of incidence, resulting in an angle-dependent phase profile. Comparing their efficiencies at the design wavelength of 530 nm [see the horizontal dashed line in Figs. 1(d)–1(f)], it is obvious that the metalens has higher efficiency over a substantially greater range of angles of incidence, while in the other cases, their peak efficiencies are lower and reduce rapidly and uniformly. Such a drawback is actually well-known as a result of the shadow effect[32] and prohibits many emerging applications. For example, in augmented reality headsets, a common configuration utilized in Microsoft HoloLens2 and Magic Leap 1 is based on guiding light into a high index substrate over a large field of view. This requires beam deflection into large angles over a wide range of angles of incidence, and therefore, those saw-tooth or multilevel prisms are obviously not suitable. Similarly, it prohibits efficient outcoupling of light from a guided mode for 3D displays.[21] In imaging, such saw-tooth Fresnel lenses and multilevel diffractive lenses have more severe vignetting (a reduction of an image's brightness toward the edge) and lower spatial

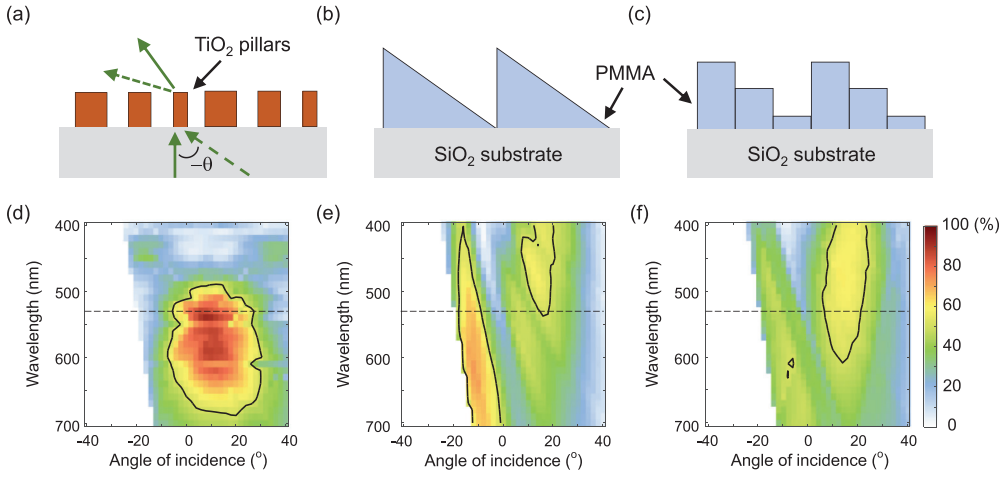

FIG. 1. Comparison of metalens, saw-tooth Fresnel lens, and multilevel diffractive lens. (a)–(c) Cross sections of typical building blocks of metalens, saw-tooth Fresnel lens, and multilevel diffractive lens, respectively. These lenses have a numerical aperture of 0.5 and were designed at $\lambda = 530$ nm at normal incidence. The TiO_2 nanopillar diameters are 230, 185, and 145 nm separated with a center-to-center distance of 350 nm. The height of TiO_2 pillars is 600 nm. The height and side of the miniature PMMA prism in (b) are 1.086 μm and 1.05 μm. The height of the miniature prism is digitized to three height levels, leading to three phase delays shown in (c). (d)–(f) Colormaps showing simulated efficiencies for (a)–(c). The efficiency was obtained by the average of x- (TM) and y-polarized (TE) incidence. The contour black lines mark 50% efficiency. The angle of incidence θ is depicted in (a).

resolution at the edge of a field.[33] On the other hand, the metalens in Fig. 1(a) has narrower spectral efficiency than the saw-tooth Fresnel lens and multilevel diffractive lenses. This is because the effective indices of pillars vary faster than the index of refraction of PMMA. Typically, the effective index of a 250 nm-diameter nanopillar changes by 0.5 from the wavelength of $\lambda = 450$ nm and 700 nm, while the index of refraction of PMMA only changes by 0.02. It is worth mentioning that nowadays, high-end monochromatic lenses are becoming more demanding for Lidar and facile recognition. For these applications, low spectral bandwidth is less problematic because the illumination sources are lasers or narrow-band light-emitting diodes. A recent article also gave an informative comparison between metalenses and diffractive lenses, including topics on optical property, large-scale fabrication, tunability, etc.[34]

It is also worth mentioning that there is room for improvement for the three different types of lenses. The bottleneck of the low spectral efficiency bandwidth in metalenses can be tackled by engineering the dispersion of constituent nanostructures.[35,36] This can be pursued by further engineering the shape of nanostructure or by topology optimization and inverse design.[37] To overcome the limitation of angular bandwidth in saw-tooth Fresnel lenses and multilevel diffractive lenses, one can cover the lenses with a layer of another polymer,[38] so that the refractive index contrast reduces and so does the shadow effect. However, this introduces another challenge that the saw-tooth patterns need to be higher in order to cover phase delays from 0 to 2π for maintaining high efficiency, leading to fabrication difficulties. So far, the limitations of spectral and angular bandwidths fundamentally result from the dispersive characteristic of effective index in metalens' constituent nanostructures and different high levels used in Fresnel lenses and multilevel diffractive lenses, respectively. An interesting question to ask is whether there is a flat lens that utilizes the material index of refraction and constant height to maintain high spectral and angular efficiencies. Indeed, existing for a long time, a liquid crystal lens consists of layers of rotated liquid crystal molecules, which has been demonstrated with both high angular and spectral efficiencies.[39] However, such lenses impart phase delay based on the Pancharatnam–Berry phase, and therefore, they are sensitive to polarization (can only focus an incident circularly polarized light, while becomes a diverging lens for another incident helicity). Although stacking four Pancharatnam–Berry liquid crystal lenses can solve the challenge of polarization sensitivity, it leads to difficulties in alignment.[40] Additionally, the manufacturing process of such lenses is usually based on laser interference instead of industrial projection lithography used in chip foundries.

We have mentioned that the dispersive characteristic of the nanostructure is much stronger than material dispersion. Such strong dispersion can be an advantage if it is considered in design. One example is an achromatic metalens that focuses the entire visible spectrum for any incident polarization [see Fig. 2(a)].[36] Its nanostructures are coupled TiO_2 nanofins, and each nanostructure's group delay (first order derivative of the phase with angular frequency), group delay dispersion (second order derivative of phase with angular frequency), and the rest high orders are engineered in the visible region, leading to a frequency-dependent phase profile,

$$\varphi(r,\omega) = -\frac{\omega}{c}\left(\sqrt{r^2+f^2}-f\right), \tag{2}$$

where ω, c, r, and f are the angular frequency, light speed, and lens radial coordinate, and focal length, respectively. Such a frequency-dependent phase profile has been realized by nanostructures of various materials in the visible and the near-infrared regions.[41–44] For verifying achromatic metalenses, the measurement of the point spread function for incident wavelengths is essential [see Fig. 2(b) for a typical measurement result for an TiO_2 achromatic metalens]. This is because the point spread

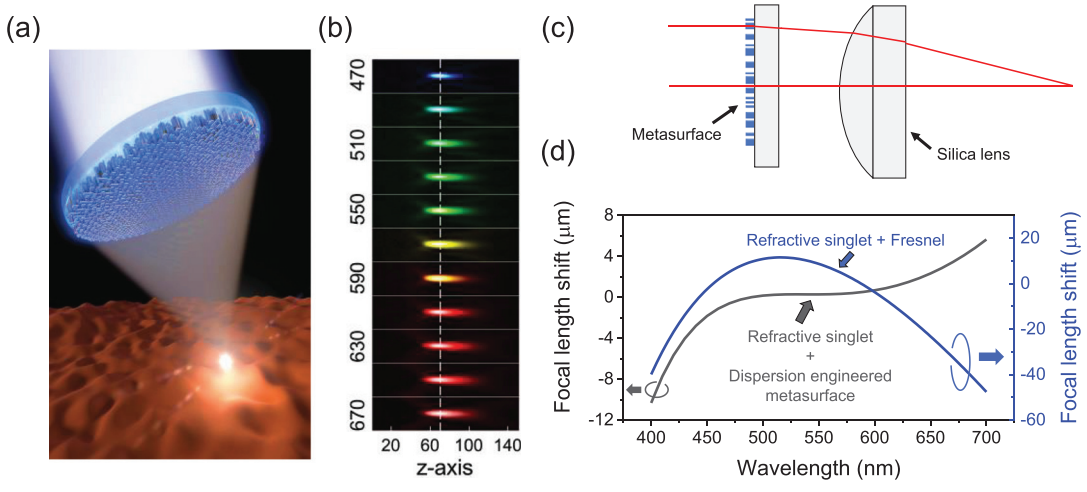

FIG. 2. Achromatic metalens and dispersion-engineered metasurface. (a) Schematic diagram of an achromatic TiO_2 metalens capable of focusing the entire visible spectrum. (b) Experimental results of the point spread function of an achromatic metalens. Colors represent incident wavelengths (labeled on the left in units of nanometer) in the visible. (c) A hybrid metasurface-refractive lens. The nanostructures (shown by blue rectangles) on the metasurface were designed with a customized phase, group delay, and group delay dispersion to correct spherical and chromatic aberrations. (d) A focal length shift comparison for the hybrid metalens and a corresponding conventional diffractive-refractive lens. They have the same diameter and numerical aperture. Note that the focal length shift of the hybrid metalens (black line) is about 5 times smaller than that of the diffractive-refractive lens. Panel (b) adapted with permission from Chen *et al.*, "A broadband achromatic metalens for focusing and imaging in the visible," Nat. Nanotechnol. **13**, 220–226 (2018). Copyright 2018 Springer Nature.

function provides information on the focal length and depth of focus and whether an achromatic metalens has multi-foci. An achromatic metalens designed following Eq. (2) is diffraction-limited and achromatic, meaning that its depth of focus is given by λ/NA^2 when NA is small and has no multiple focal spots. Recently, achromatic metalenses have been demonstrated with different materials for applications in wavelength regions.[6] However, these achromatic metalens singlets are limited by the product of the diameter and NA. For achromatic metalenses in the visible of NA = 0.2, their diameters are usually smaller than 30 μm because the nanostructures can only provide a limited range of group delay, while the required group delay of the achromatic metalens given by Eq. (2) increases rapidly with diameter. To overcome this limitation, one can cascade a dispersion-engineered metasurface with a refractive singlet such that the hybrid metasurface-refractive lens is achromatic and diffraction-limited in the visible [see the schematic in Fig. 2(c)].[53] The uniqueness of such a hybrid metasurface-refractive lens is its superior achromatic bandwidth compared with a conventional counterpart consisting of a diffractive lens and the same refractive singlet [see the black and blue curves in Fig. 2(d)]. Conventional diffractive-refractive lens doublets (a diffractive lens with a refractive singlet) can only have two wavelengths being focused on the same plane, leading to a significant secondary spectrum.[45] Such a secondary spectrum is corrected in the hybrid metasurface-refractive lens shown by the black curve in Fig. 2(d). This is because the group delay dispersion was taken into account, which corrects the secondary spectrum.

Nowadays, there are many applications related to monochromatic light based on lasers, such as Lidar and depth sensing. We will introduce two examples: a full-Stokes polarization camera[46] and a metalens depth sensor.[47] The first example is a metalens full-Stokes camera shown in Fig. 3(a). Unlike the most, if not all, commercial polarization cameras, which can only observe linearly polarized information,[48] the metalens full-Stokes camera is capable of analyzing the Stokes vector of all elements. In particular, this metalens full-Stokes polarization camera has no moving part and, therefore, can analyze polarization information with a speed mainly determined by the frame rate of the camera sensor. The key element of the metalens polarization camera is the metasurface that diffracts incident polarization to four quadrants with given polarization states, shown in the top-right inset in Fig. 3(a). By measuring the intensity on these diffraction orders, incident polarization can be retrieved using a Stokes polarimetry. By superimposing the images (quadrants) of the scene analyzed by the four diffraction orders, the polarization of each pixel of the scene is retrieved.[46] For instance, the first row of Fig. 3(b) shows an acrylic plate before and after applying pressure by hand. From their intensity images (S_0, second row), there is no difference, while they show a significant stress-induced polarization change in S_3 (the last row).

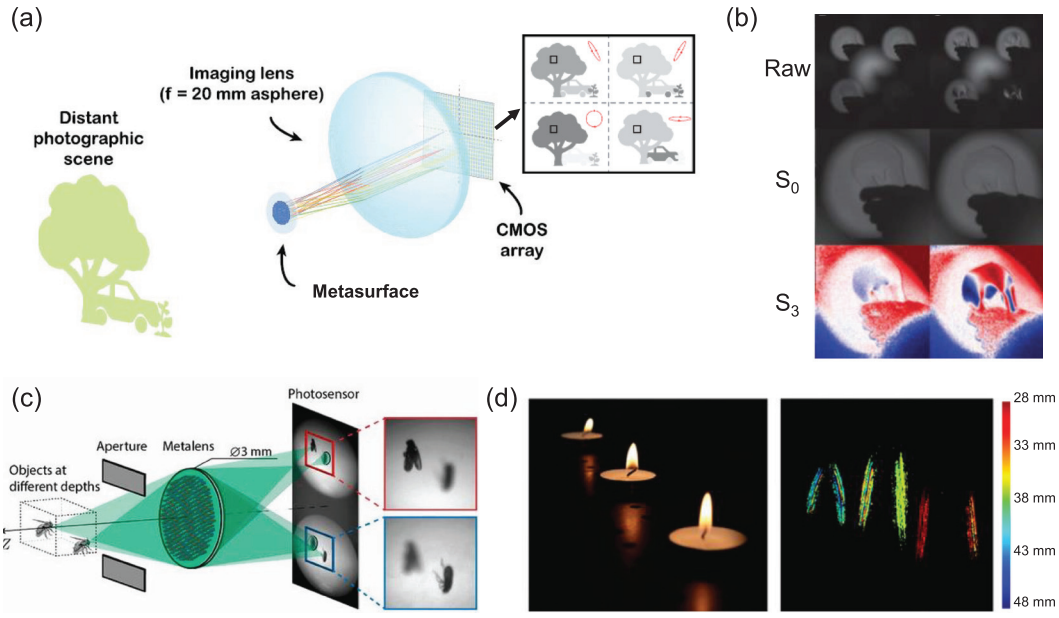

FIG. 3. Metasurface full-Stokes polarization camera and metalens depth sensor. (a) Schematic diagram of a full-Stokes polarization camera consisting of only three components: a metasurface, a lens, and a camera sensor. The metasurface replicates four separate images on the quadrants of the sensor corresponding to the scene analyzed by the polarization associated with the four diffraction orders, as shown by the inset in the top right corner. (b) Polarization images where the first row shows raw data. Note that the center blur spot results from zeroth order diffraction of the metasurface. After a postprocessing, one can obtain the intensity (S_0: the second row) and the S_3 Stokes parameter pixel by pixel, which provides information on the amount of circular polarization. The sample is an acrylic plate. After squeezing it (second column), stress-induced birefringence appears, which is invisible in S_0 images. (c) Schematic of a metalens depth sensor inspired by jumping spider. The metalens focuses the light off-axis and has dual focal lengths. As a result, a fruit fly placed at a given z distance forms images with different amounts of blurriness. Using a simple equation that contains the intensity difference between the images and the Laplacian of the sum of their intensities, the position of the fly can be determined. (d) An interesting example of sensing the positions of candle flames using the metalens depth sensor. Left panel: photograph of the candle sample taken using a commercial camera. Right panel: depth map of candle flames. Panels (a) and (b) adapted with permission from Shaltout *et al.*, "Spatiotemporal light control with frequency-gradient metasurfaces," Science **365**, eaax1839 (2019). Copyright 2019 American Association for the Advancement of Science.

The second example of a metalens depth camera (a depth sensor) is schematically shown in Fig. 3(c) and was inspired by jumping spiders.[47] Jumping spider's primary eyes have four layers of retinas.[49] When it captures the prey, its brain processes the images using the retinas with different amounts of defocusing, which provides depth information. The metalens was designed to mimic this principle by using two focal lengths, which form two images on the sensor. As a result, when an object [schematically shown by the flies in Fig. 3(c)] is imaged by the metalens, two images with different amounts of blurriness are formed. We then can calculate the depth map based on an efficient image processing algorithm and a simple formula that links the distance to the blurriness, which makes a significant difference in comparison with approaches based on the microlens array.[50,51] Note that the metalens depth sensor can also provide depth information for low reflectivity objects. As a demonstration, three candles were placed along the optical axis at different distances [left panel in Fig. 3(d)] and their distances were distinguished as shown in the right panel.

In summary, metasurfaces promise a major reduction in the footprint and system complexity and new optical functionalities. We have introduced the advantages of metasurface technology and highlighted achromatic metasurface components, a metasurface full-Stokes camera and a metasurface depth sensor. The achromatic metasurface components were designed based on dispersion engineering, which, according to our perspective, is an emerging and important research topic for further study.[52] In addition, to bring metasurface components into consumer devices, fast-developing projection lithography (critical dimension was 130 nm two decades ago to nowadays 5 nm) has been demonstrated for mass producing metasurface components on a 12-inch wafer.[15] We envision this as a unique opportunity of potentially unifying two industries: semiconductor manufacturing and lens-making for disruptive products and applications. With global coherent efforts from academia, industry, and government agencies (a few examples were quoted in this article), we foresee that metasurface components will soon appear in everyday life in the coming years.

This work was supported by the Air Force Office of Scientific Research under Grant Nos. FA9550-18-P-0024, FA9550-16-1-0156, and FA9550-14-1-0389 (MURI) and National Science Foundation Award (Grant No. IIS-1718012).

DATA AVAILABILITY

The data that support the findings of this study are available from the corresponding author upon reasonable request.

REFERENCES

[1]N. Yu, P. Genevet, M. A. Kats, F. Aieta, J.-P. Tetienne, F. Capasso, and Z. Gaburro, "Light propagation with phase discontinuities: generalized laws of reflection and refraction," Science **334**, 333–337 (2011).
[2]X. Luo, "Engineering optics 2.0: A revolution in optical materials, devices, and systems," ACS Photonics **5**, 4724–4738 (2018).
[3]G.-Y. Lee, G. Yoon, S.-Y. Lee, H. Yun, J. Cho, K. Lee, H. Kim, J. Rho, and B. Lee, "Complete amplitude and phase control of light using broadband holographic metasurfaces," Nanoscale **10**, 4237–4245 (2018).
[4]A. H. Dorrah, N. A. Rubin, A. Zaidi, M. Tamagnone, and F. Capasso, "Metasurface optics for on-demand polarization transformations along the optical path," Nat. Photonics (in press) (2021).
[5]S. M. Kamali, E. Arbabi, A. Arbabi, and A. Faraon, "A review of dielectric optical metasurfaces for wavefront control," Nanophotonics **7**, 1041 (2018).
[6]W. T. Chen, A. Y. Zhu, and F. Capasso, "Flat optics with dispersion-engineered metasurfaces," Nat. Rev. Mater **5**, 604–620 (2020).
[7]M. Khorasaninejad and F. Capasso, "Metalenses: Versatile multifunctional photonic components," Science **358**, eaam8100 (2017).
[8]A. M. Shaltout, K. G. Lagoudakis, J. van de Groep, S. J. Kim, J. Vučković, V. M. Shalaev, and M. L. Brongersma, "Spatiotemporal light control with frequency-gradient metasurfaces," Science **365**, 374–377 (2019).
[9]M. Henstridge, C. Pfeiffer, D. Wang, A. Boltasseva, V. M. Shalaev, A. Grbic, and R. Merlin, "Synchrotron radiation from an accelerating light pulse," Science **362**, 439–442 (2018).
[10]L. Li, Z. Liu, X. Ren, S. Wang, V.-C. Su, M.-K. Chen, C. H. Chu, H. Y. Kuo, B. Liu, W. Zang, G. Guo, L. Zhang, Z. Wang, S. Zhu, and D. P. Tsai, "Metalens-array–based high-dimensional and multiphoton quantum source," Science **368**, 1487–1490 (2020).
[11]J.-S. Park, S. Zhang, A. She, W. T. Chen, P. Lin, K. M. A. Yousef, J.-X. Cheng, and F. Capasso, "All-glass, large metalens at visible wavelength using deep-ultraviolet projection lithography," Nano Lett. **19**, 8673–8682 (2019).
[12]G. Yoon, K. Kim, D. Huh, H. Lee, and J. Rho, "Single-step manufacturing of hierarchical dielectric metalens in the visible," Nat. Commun. **11**, 2268 (2020).
[13]R. C. Devlin, M. Khorasaninejad, W. T. Chen, J. Oh, and F. Capasso, "Broadband high-efficiency dielectric metasurfaces for the visible spectrum," Proc. Natl. Acad. Sci. U.S.A. **113**, 10473–10478 (2016).
[14]A. Arbabi, Y. Horie, M. Bagheri, and A. Faraon, "Dielectric metasurfaces for complete control of phase and polarization with subwavelength spatial resolution and high transmission," Nat. Nanotechnol. **10**, 937–943 (2015).
[15]T. Hu, C.-K. Tseng, Y. H. Fu, Z. Xu, Y. Dong, S. Wang, K. H. Lai, V. Bliznetsov, S. Zhu, Q. Lin, and Y. Gu, "Demonstration of color display metasurfaces via immersion lithography on a 12-inch silicon wafer," Opt. Express **26**(15), 19548–19554 (2018).
[16]Z. Xu, Y. Dong, C.-K. Tseng, T. Hu, J. Tong, Q. Zhong, N. Li, L. Sim, K. H. Lai, Y. Lin, D. Li, Y. Li, V. Bliznetsov, Y.-H. Fu, S. Zhu, Q. Lin, D. H. Zhang, Y. Gu, N. Singh, and D.-L. Kwong, "CMOS-compatible all-Si metasurface polarizing bandpass filters on 12-inch wafers," Opt. Express **27**, 26060–26069 (2019).
[17]See https://www.osa.org/en-us/meetings/incubator_meetings/2020/flatopticsinc/ for "OSA Incubator Meeting on Flat Optics" (last accessed December 6, 2020).
[18]See https://www.sait.samsung.co.kr/saithome/about/collabo_apply.do for "Samsung Global Collaboration" (last accessed February 8, 2020).
[19]See https://www.sony.com/research-award-program#FocusedResearchAward for "SONY Research Award Program" (last accessed February 8, 2020).
[20]G. Akselrod, "Optics for automotve LiDAR: Metasurface beam steering enables solid- state, high-performance LiDAR," LaserFocusedWorld (2019), available at https://www.laserfocusworld.com/optics/article/14036818/metasurface-beam-steering-enables-solidstate-highperformance-lidar.
[21]D. Fattal, Z. Peng, T. Tran, S. Vo, M. Fiorentino, J. Brug, and R. G. Beausoleil, "A multi-directional backlight for a wide-angle, glasses-free three-dimensional display," Nature **495**, 348–351 (2013).
[22]See https://www.metalenz.com/ for "Metalez Inc."
[23]See https://metamaterial.com/ for "Metamaterial Technologies."
[24]See https://www.luxresearchinc.com/press-releases/lux-research-forecasts-10.7-billion-market-opportunity-in-metamaterial-devices for "Lux Research: Metamaterials Market Forecast" (last accessed Feburary 8, 2020).
[25]S. J. Byrnes, A. Lenef, F. Aieta, and F. Capasso, "Designing large, high-efficiency, high-numerical-aperture, transmissive meta-lenses for visible light," Opt. Express **24**, 5110–5124 (2016).
[26]S. Banerji, M. Meem, A. Majumder, F. G. Vasquez, B. Sensale-Rodriguez, and R. Menon, "Imaging with flat optics: Metalenses or diffractive lenses?," Optica **6**, 805–810 (2019).
[27]D. A. Buralli and G. M. Morris, "Design of a wide field diffractive landscape lens," Appl. Opt. **28**, 3950–3959 (1989).
[28]B. Groever, W. T. Chen, and F. Capasso, "Meta-lens doublet in the visible region," Nano Lett. **17**, 4902–4907 (2017).
[29]A. Arbabi, E. Arbabi, S. M. Kamali, Y. Horie, S. Han, and A. Faraon, "Miniature optical planar camera based on a wide-angle metasurface doublet corrected for monochromatic aberrations," Nat. Commun. **7**, 13682 (2016).
[30]X. Zhang, Q. Li, F. Liu, M. Qiu, S. Sun, Q. He, and L. Zhou, "Controlling angular dispersions in optical metasurfaces," Light Sci. Appl. **9**, 76 (2020).

[31]L. Wenwei, L. Zhancheng, C. Hua, T. Chengchun, L. Junjie, Z. Shuang, C. Shuqi, and T. Jianguo, "Metasurface enabled wide-angle Fourier lens," Adv. Mater. **30**, 1706368 (2018).
[32]P. Lalanne and P. Chavel, "Metalenses at visible wavelengths: Past, present, perspectives," Laser Photonics Rev. **11**, 1600295 (2017).
[33]M. Decker, W. T. Chen, T. Nobis, A. Y. Zhu, M. Khorasaninejad, Z. Bharwani, F. Capasso, and J. r Petschulat, "Imaging performance of polarization-insensitive metalenses," ACS Photonics **6**, 1493–1499 (2019).
[34]J. Engelberg and U. Levy, "The advantages of metalenses over diffractive lenses," Nat. Commun. **11**, 1991 (2020).
[35]W. T. Chen, A. Y. Zhu, J. Sisler, Z. Bharwani, and F. Capasso, "A broadband achromatic polarization-insensitive metalens consisting of anisotropic nanostructures," Nat. Commun. **10**, 355 (2019).
[36]W. T. Chen, A. Y. Zhu, V. Sanjeev, M. Khorasaninejad, Z. Shi, E. Lee, and F. Capasso, "A broadband achromatic metalens for focusing and imaging in the visible," Nat. Nanotechnol. **13**, 220–226 (2018).
[37]T. Phan, D. Sell, E. W. Wang, S. Doshay, K. Edee, J. Yang, and J. A. Fan, "High-efficiency, large-area, topology-optimized metasurfaces," Light Sci. Appl. **8**, 48 (2019).
[38]D. Werdehausen, S. Burger, I. Staude, T. Pertsch, and M. Decker, "Dispersion-engineered nanocomposites enable achromatic diffractive optical elements," Optica **6**, 1031–1038 (2019).
[39]M. J. Escuti, J. Kim, and M. W. Kudenov, "Controlling light with geometric-phase holograms," Opt. Photonics News **27**, 22–29 (2016).
[40]T. Zhan, J. Xiong, Y.-H. Lee, and S.-T. Wu, "Polarization-independent Pancharatnam-Berry phase lens system," Opt. Express **26**, 35026–35033 (2018).
[41]S. Wang, P. C. Wu, V.-C. Su, Y.-C. Lai, M.-K. Chen, H. Y. Kuo, B. H. Chen, Y. H. Chen, T.-T. Huang, J.-H. Wang, R.-M. Lin, C.-H. Kuan, T. Li, Z. Wang, S. Zhu, and D. P. Tsai, "A broadband achromatic metalens in the visible," Nat. Nanotechnol. **13**, 227–232 (2018).
[42]E. Arbabi, A. Arbabi, S. M. Kamali, Y. Horie, and A. Faraon, "Controlling the sign of chromatic dispersion in diffractive optics with dielectric metasurfaces," Optica **4**, 625–632 (2017).
[43]S. Shrestha, A. C. Overvig, M. Lu, A. Stein, and N. Yu, "Broadband achromatic dielectric metalenses," Light Sci. Appl. **7**, 85 (2018).
[44]A. Ndao, L. Hsu, J. Ha, J.-H. Park, C. Chang-Hasnain, and B. Kanté, "Octave bandwidth photonic fishnet-achromatic-metalens," Nat. Commun. **11**, 3205 (2020).
[45]J. M. Geary, *Introduction to Lens Design: With Practical ZEMAX Examples*, Introduction to Lens Design: With Practical ZEMAX Examples (Willmann-Bell, Richmond, 2002).
[46]N. A. Rubin, G. D'Aversa, P. Chevalier, Z. Shi, W. T. Chen, and F. Capasso, "Matrix Fourier optics enables a compact full-Stokes polarization camera," Science **365**, eaax1839 (2019).
[47]Q. Guo, Z. Shi, Y.-W. Huang, E. Alexander, C.-W. Qiu, F. Capasso, and T. Zickler, "Compact single-shot metalens depth sensors inspired by eyes of jumping spiders," Proc. Natl. Acad. Sci. U.S.A. **116**(46), 22959–22965 (2019).
[48]See https://www.sony-semicon.co.jp/e/products/IS/industry/technology/polarization.html for "Sony Polarization Cameras."
[49]T. Nagata, M. Koyanagi, H. Tsukamoto, S. Saeki, K. Isono, Y. Shichida, F. Tokunaga, M. Kinoshita, K. Arikawa, and A. Terakita, "Depth perception from image defocus in a jumping spider," Science **335**, 469–471 (2012).
[50]R. J. Lin, V.-C. Su, S. Wang, M. K. Chen, T. L. Chung, Y. H. Chen, H. Y. Kuo, J.-W. Chen, J. Chen, Y.-T. Huang, J.-H. Wang, C. H. Chu, P. C. Wu, T. Li, Z. Wang, S. Zhu, and D. P. Tsai, "Achromatic metalens array for full-colour light-field imaging," Nat. Nanotechnol. **14**, 227–231 (2019).
[51]B. H. Chen, P. C. Wu, V.-C. Su, Y.-C. Lai, C. H. Chu, I. C. Lee, J.-W. Chen, Y. H. Chen, Y.-C. Lan, and C.-H. Kuan, "GaN metalens for pixel-level full-color routing at visible light," Nano Lett. **17**, 6345–6352 (2017).
[52]C. Caloz, "Tomorrow's metamaterials: Manipulation of electromagnetic waves in space, time and spacetime," arXiv preprint 1602.04340 (2016).
[53]W. T. Chen, A. Y. Zhu, J. Sisler, Y.-W. Huang, K. M. A. Yousef, E. Lee, C.-W. Qiu, and F. Capasso, "Broadband achromatic metasurface-refractive optics," Nano Lett. **18**, 7801–7808 (2018).